

Formation of Organic Ion Cocrystals, Phase Transition and Ion Conduction

Yin Qian,^{*a} Yi-Ming Wang,^a Lei Xu,^a Wan-Wan Yao,^a Dong-Sheng Shao,^a Xiao-Ming Ren^{* a,b}

^a State Key Laboratory of Materials-Oriented Chemical Engineering and College of Chemistry and Molecular Engineering, Nanjing Tech University, Nanjing 211816, P. R. China

^b State Key Laboratory of Coordination Chemistry, Nanjing University 210023, P. R. China

Tel: 86-25-58139476

E-mail: yinqian@njtech.edu.cn (YQ); xmren@njtech.edu.cn (XMR)

Contents

Experimental section

Reagents and materials

Preparation of compounds

Physical measurements

X-ray Crystallography

Table S1. Crystallographic data and structure refinements for **Me, Et, Pr** and **Bu**

Table S2. Crystallographic data and structure refinements for **MeEt, MeBu** and **EtBu**

Details of first principles total energy calculation for crystals using DFT method

Figure S1: IR spectra of (a–c) **Me, Et, Pr** and **Bu**, (d–f) **Me, Et** and **MeEt**, (g–i) **Me, Bu** and **MeBu**, (j–l) **Et, Bu** and **EtBu**.

Table S3. Main vibrational bands and assignments in IR spectra of **Me, Et, Pr, Bu, MeEt, MeBu** and **EtBu**

Figure S2: TG plots of (a, b) **Me, Et** and **MeEt**; (c) **Me, Bu** and **MeBu**; (d) **Et, Bu** and **EtBu**.

Figure S3. Experimental and simulated PXRD patterns of (a) **Me**, (b) **Et**, (c) **Pr**, (d) **Bu**. The simulated PXRD patterns of four salts are obtained from the corresponding single crystal diffraction data by Mercury 3.1 program. Experimental pattern matches well with the corresponding simulated one for each salt.

Figure S4. PXRD patterns of (a) **Me, Et** and **MeEt** (b) **Me, Bu** and **MeBu** (c) **Et, Bu** and **EtBu**. And experimental and simulated PXRD patterns of (d) **MeEt** (e) **MeBu** (f) **EtBu**. The simulated PXRD patterns of three co-crystals are acquired from the corresponding single crystal diffraction data by Mercury 3.1 program. Experimental pattern matches well with the corresponding simulated one for each co-crystal.

Figure S5. PXRD patterns of (a) **Me, Pr** and **Me+Pr** (b) **Et, Pr** and **Et+Pr** (c) **Pr, Bu** and **Pr+Bu**, in which **Me+Pr** represents the crystalline sample obtained by slow evaporation the solution of **Me** and **Pr** with equal mole ratio; the symbols, **Et+Pr** and **Pr+Bu**, show similar meanings, and the details refer to the main text.

Figure S6. (a) Asymmetric unit (where the displacement ellipsoids are drawn at 50% probability level for non-hydrogen atoms, and hydrogen atoms are omitted for clarity), and packing diagrams of viewed along (b) a-axis (c) b-axis (d) c-axis for **Me**.

Figure S7. (a) Asymmetric unit (where the displacement ellipsoids are drawn at 50% probability level for non-hydrogen atoms, and hydrogen atoms are omitted for clarity), and packing diagrams of viewed along (b) a-axis (c) b-axis (d) c-axis for **Et**.

Figure S8. (a) Asymmetric unit (where the displacement ellipsoids are drawn at 50% probability level for non-hydrogen atoms, and hydrogen atoms are omitted for clarity), and packing diagrams of viewed along (b) a-axis (c) b-axis (d) c-axis for **Et**.

Figure S9. Packing diagrams of viewed along (a) b-axis and (d) c-axis for **Pr**.

Figure S10. Packing diagrams in **MeEt** viewed along (a) a-axis and (b) b-axis; (c) anion monolayer in **MeEt** viewed along a-axis.

Figure S11. Packing diagrams of viewed along (a) c-axis and (d) b-axis for **MeBu**.

Figure S12. Packing diagrams of viewed along (a) b-axis and (b) c-axis for **EtBu**.

Figure S13. Plots of (a) van der Waals volume per cation, which was obtained by PLATON program, in (a) **Me**, **Et**, **Pr** and **Bu**; (b) Me_4N^+ in **Me**, **MeEt**, **MeBu**; (c) Et_4N^+ in **Et**, **MeEt** and **EtBu**; (d) Bu_4N^+ in **Bu**, **MeBu** and **EtBu**.


Figure S14. Plots of $V_{\text{f.u.}}$ and $E_{\text{Latt/f.u.}}$ against formula weight for **Me**, **Et**, **Pr**, **Bu**, **MeEt**, **MeBu** and **EtBu**, where the green diamond  in two plots represent the $V_{\text{f.u.}}$ and $E_{\text{Latt/f.u.}}$ of **Pr**.

Table S4. Comparison of crystal volume per formula unit and crystal energy per formula unit of a cocrystal with its two corresponding salts

Figure S15. Variable temperature crystal morphologies of **Me**, **Et**, **Pr**, **MeEt**, **MeBu** and **EtBu**.

Figure S16. Impedances at 358 K together with the corresponding fit curves using the equivalent circuit (insets) for (a) **Me**, (b) **Et**, (c) **Bu**, (d) **MeEt**, (e) **MeBu** and (f) **EtBu**.

Figure S17. Impedances at 433 K together with the corresponding fit curves using the equivalent circuit (inset) for (a) **Me**, (b) **Et**, (c) **Bu**, (d) **MeEt**, (e) **MeBu** and (f) **EtBu**.

Figure S18. Arrhenius plots together with the corresponding linear fits and activation energies for (a) **Me**, (b) **Et**, (c) **MeEt**, (d) **MeBu** and (e) **EtBu**.

References

Experimental section

Reagents and materials

All reagents and materials are of analytical grade and used as received from commercial sources without any further purification. Tetramethylammonium bromide (Me_4NBr), tetraethylammonium bromide (Et_4NBr), tetrapropylammonium bromide (Pr_4NBr), tetrabutylammonium bromide (Bu_4NBr) are products of Macklin chemicals and Disodium maleonitriledithiolate (Na_2mnt) was prepared following the procedures published.¹

Preparation of compounds

$[\text{Me}_4\text{N}]_2[\text{Ni}(\text{mnt})_2]$ (Me). A mixture of $\text{NiCl}_2 \cdot 6\text{H}_2\text{O}$ (0.237 g, 0.01 mol), Na_2mnt (0.37 g, 0.02 mol) and Me_4NBr (0.383 g, 0.2 mol) in solution of H_2O was stirred for 2 h. The red microcrystals formed were filtered off, washed with H_2O and dried under vacuum. Single crystals of $[\text{Me}_4\text{N}]_2[\text{Ni}(\text{mnt})_2]$ were gained by evaporating in MeCN solution at room temperature. Yield: more than 90%.

$[\text{Et}_4\text{N}]_2[\text{Ni}(\text{mnt})_2]$ (Et), $[\text{Bu}_4\text{N}]_2[\text{Ni}(\text{mnt})_2]$ (Bu) and $[\text{Pr}_4\text{N}]_2[\text{Ni}(\text{mnt})_2]$ (Pr). A similar process was used for preparation of **Et**, **Bu** and **Pr** crystals, just replacing the reactant Me_4NBr with Et_4NBr , Pr_4NBr and Bu_4NBr , respectively. Yield: 89% for **Et**, 85% for **Bu** and 92% for **Pr**.

The crystal structure data were previously reported for $[\text{Me}_4\text{N}]_2[\text{Ni}(\text{mnt})_2]$,² $[\text{Et}_4\text{N}]_2[\text{Ni}(\text{mnt})_2]$ ³ and $[\text{Bu}_4\text{N}]_2[\text{Ni}(\text{mnt})_2]$,³ and re-determined in this study.

$[\text{Me}_4\text{N}][\text{Et}_4\text{N}][\text{Ni}(\text{mnt})_2]$ (MeEt), $[\text{Me}_4\text{N}][\text{Bu}_4\text{N}][\text{Ni}(\text{mnt})_2]$ (MeBu) and $[\text{Et}_4\text{N}][\text{Bu}_4\text{N}][\text{Ni}(\text{mnt})_2]$ (EtBu). The co-crystals were obtained using the similar procedure, and herein, the process for growth of $[\text{Me}_4\text{N}][\text{Et}_4\text{N}][\text{Ni}(\text{mnt})_2]$ co-crystals is described in details.

$[\text{Me}_4\text{N}]_2[\text{Ni}(\text{mnt})_2]$ (487 mg, 1 mmol) and $[\text{Et}_4\text{N}]_2[\text{Ni}(\text{mnt})_2]$ (600 mg, 1 mmol) were mixed and dissolved in 25 mL of MeCN and EtOH mixed solution ($V_{\text{MeCN}}: V_{\text{EtOH}} = 4:1$). The mixture was stirred for 20 min at ambient temperature and filtered, and the filtrate was evaporated at ambient condition for two days and until only less than 1 mL of solution was left, and the crystals of **MeEt** were collected, washed using

1 mL of MeOH and dried in air. Yield: 69% for **MeEt**, 62% for **MeBu** and 75% for **EtBu**.

Physical measurements

Elemental analyses for C, H and N were performed with an Elementar Vario EL III analytic instrument. Infrared spectra (IR) were recorded on a Nicolet iS5 spectrometer with KBr pellets in the spectral regime of 400-4000 cm^{-1} . Powder X-ray diffraction data were collected using a SHIMADZU XRD-6100 diffractometer with $\text{Cu K}\alpha$ radiation ($\lambda = 1.5418 \text{ \AA}$), operated at 40 kV and 40 mA, and the 2θ angle ranges from 5 to 50° with a step of 0.01° at ambient condition. Thermogravimetric analysis (TGA) was performed with a SDT Q600 thermogravimetric analyzer in 20–800 $^\circ\text{C}$ under nitrogen atmosphere; the polycrystalline sample was placed in a platinum-pan, the heating rate is 20 $^\circ\text{C min}^{-1}$ and the nitrogen flow rate is 100 mL min^{-1} . Differential scanning calorimetry (DSC) was carried out on a Pyris 1 power-compensation differential scanning calorimeter with a warming rate of 10 K min^{-1} during the heating process. Optical photographs were taken with a Leica DMRX polarizing optical microscope equipped with an LINKAM LTS350 cool and hot stage.

X-ray Crystallography

Single crystal X-ray diffraction (SCXRD) data were collected using Graphite monochromated $\text{Mo K}\alpha$ ($\lambda = 0.71073 \text{ \AA}$) on a Bruker D8 QUEST Apex II CCD area detector diffractometer. Data reduction and absorption correction were performed with the SAINT⁴ and SADABS⁵ software packages, respectively. The structures were solved by a direct method using the SHELXL-2018 software package.⁶ The non-hydrogen atoms were anisotropically refined using the full-matrix least-squares method on F^2 . All hydrogen atoms were geometrically fixed and placed in ideal position. Crystallographic data and structure refinements are listed in Table S1 and S2.

Table S1. Crystallographic data and structure refinements for **Me, Et, Pr** and **Bu**

Compound	Me	Et	Pr	Bu
Temperature / K	296	293	296	273
Chemical formula	C ₁₆ H ₂₄ N ₆ NiS ₄	C ₂₄ H ₄₀ N ₆ NiS ₄	C ₃₂ H ₅₆ N ₆ NiS ₄	C ₄₀ H ₇₂ N ₆ NiS ₄
CCDC number	2076768	2076767	2076766	2008198
Formula weight	487.36	599.57	711.77	823.98
Crystal system	Triclinic	Triclinic	Monoclinic	Triclinic
Wavelength	0.71073	0.71073	0.71073	0.71073
Space group	P-1	P-1	P2 ₁ /n	P-1
<i>a</i> (Å)	8.0311(6)	7.5511(4)	10.2851(5)	9.9393(8)
<i>b</i> (Å)	9.2690(7)	8.7000(4)	12.7962(7)	10.8566(9)
<i>c</i> (Å)	9.4907(7)	12.6118(7)	15.8552(8)	12.4164(10)
α (°)	114.353(3)	86.360(2)	90	85.495(3)
β (°)	103.978(3)	75.717(2)	105.9696(12)	88.170(3)
γ (°)	100.933(3)	75.416(2)	90	64.723(2)
V(Å ³) / Z	590.19(8)/1	777.05(7)/1	2006.18(18)/2	1207.79(17)/1
ρ (g×cm ⁻³)	1.371	1.281	1.178	1.133
F(000)	254	318	764	446
θ Ranges (data collection ^o)	4.428-25.497	2.42-27.56	3.11-26	2.27-27.55
Index range	-52 ≤ <i>h</i> ≤ 54, -9 ≤ <i>k</i> ≤ 9, -36 ≤ <i>l</i> ≤ 37	-9 ≤ <i>h</i> ≤ 9, -11 ≤ <i>k</i> ≤ 11, -16 ≤ <i>l</i> ≤ 16	-12 ≤ <i>h</i> ≤ 12, -15 ≤ <i>k</i> ≤ 15, -19 ≤ <i>l</i> ≤ 17	-12 ≤ <i>h</i> ≤ 12, -12 ≤ <i>k</i> ≤ 14, -16 ≤ <i>l</i> ≤ 16
Goodness-of-fit on <i>F</i> ²	1.134	0.745	1.025	1.021
^a R ₁ , ^b wR ₂ [<i>I</i> > 2σ(<i>I</i>)]	R ₁ = 0.0505, wR ₂ = 0.1149	R ₁ = 0.0425, wR ₂ = 0.1174	R ₁ = 0.0426, wR ₂ = 0.0853	R ₁ = 0.0631, wR ₂ = 0.1280
R ₁ , wR ₂ [all data]	R ₁ = 0.0698, wR ₂ = 0.1294	R ₁ = 0.0829, wR ₂ = 0.1491	R ₁ = 0.0756, wR ₂ = 0.0945	R ₁ = 0.1753, wR ₂ = 0.1573

$$^a R_1 = \sum ||F_o| - |F_c|/\sum |F_o|; ^b wR_2 = \{\sum [w(F_o^2 - F_c^2)^2] / \sum [w(F_o^2)^2]\}^{1/2}$$

Table S2. Crystallographic data and structure refinements for **MeEt**, **MeBu** and **EtBu**

Compound	MeEt	MeBu	EtBu
Temperature / K	293	293	293
Chemical formula	C ₂₀ H ₃₂ N ₆ NiS ₄	C ₂₈ H ₄₈ N ₆ NiS ₄	C ₃₂ H ₅₆ N ₆ NiS ₄
CCDC number	2144910	2144911	2144912
Formula weight	543	656	712
Crystal system	Monoclinic	Triclinic	Monoclinic
Wavelength	0.71073	0.71073	0.71073
Space group	<i>P</i> 2 ₁ / <i>c</i>	<i>P</i> -1	<i>P</i> 2 ₁ / <i>c</i>
<i>a</i> (Å)	9.8898(7)	9.9396(4)	17.7929(9)
<i>b</i> (Å)	11.0565(8)	19.2932(8)	15.3944(8)
<i>c</i> (Å)	12.9603(9)	19.4036(8)	16.2435(8)
α (°)	90	103.9340(10)	90
β (°)	103.974(2)	94.1090(10)	116
γ (°)	90	90.7530(10)	90
<i>V</i> (Å ³) / <i>Z</i>	1375.22(17)/2	3600.4(3)/4	3991.7(4)/4
ρ (g×cm ⁻³)	1.312	1.210	1.184
F(000)	572	1400	1528
θ Ranges (data collection°)	2.45-27.59	1.084-27.574	1.924-27.606
Index range	-11 ≤ <i>h</i> ≤ 12, -11 ≤ <i>k</i> ≤ 14, -16 ≤ <i>l</i> ≤ 16	-12 ≤ <i>h</i> ≤ 12, -25 ≤ <i>k</i> ≤ 25, -25 ≤ <i>l</i> ≤ 25	-23 ≤ <i>h</i> ≤ 19, -20 ≤ <i>k</i> ≤ 19, -15 ≤ <i>l</i> ≤ 21
Goodness-of-fit on <i>F</i> ²	1.031	1.210	1.184
^a R ₁ , ^b wR ₂ [<i>I</i> >2 σ (<i>I</i>)]	R ₁ = 0.0776, wR ₂ = 0.1791	R ₁ = 0.0520, wR ₂ = 0.1027	R ₁ = 0.0635, wR ₂ = 0.1777
R ₁ , wR ₂ [all data]	R ₁ = 0.1853, wR ₂ = 0.2186	R ₁ = 0.1201, wR ₂ = 0.1221	R ₁ = 0.1597, wR ₂ = 0.2361

$$^a R_1 = \sum ||F_o| - |F_c|/\sum |F_o|; ^b wR_2 = \{\sum [w(F_o^2 - F_c^2)^2] / \sum [w(F_o^2)^2]\}^{1/2}$$

Details of first principles total energy calculation for crystals using DFT method

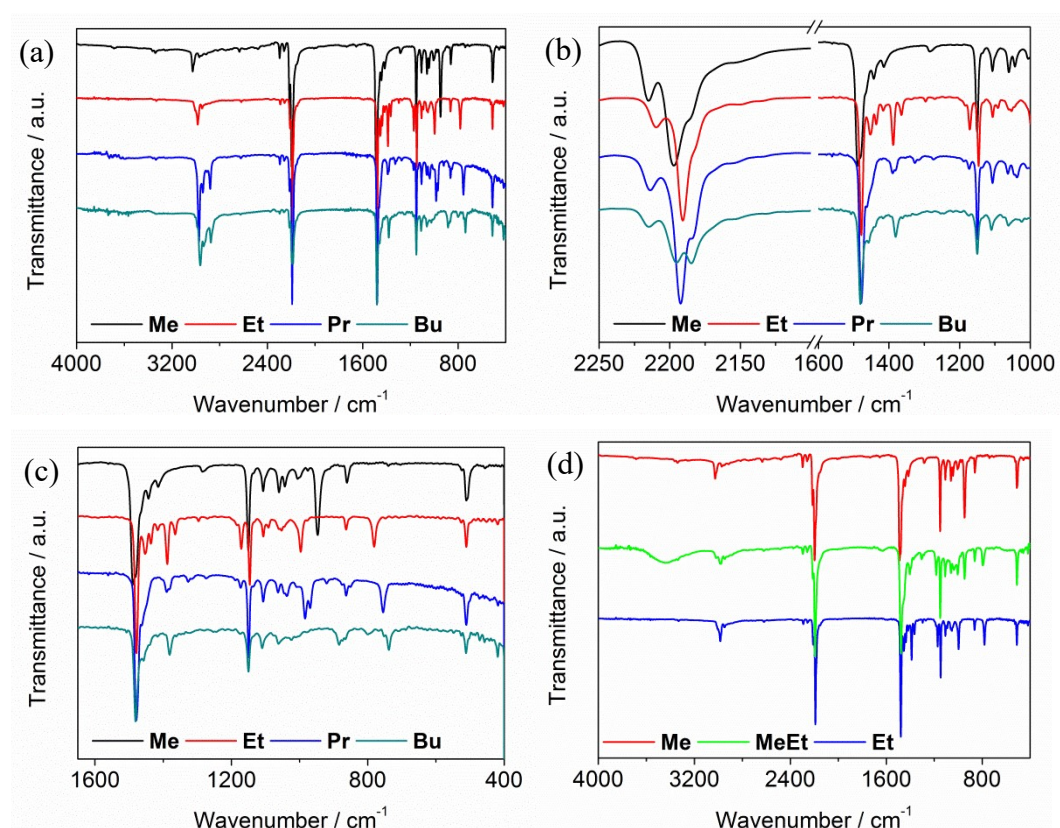
All density functional theory (DFT) calculations are performed using Dmol³ code developed by Delley.⁷ The non-modelized crystal structures were taken from X-ray single crystal structure analyses for each salt, and the atom coordinates were optimized, while the cell parameters were fixed during structural optimization. The optimized crystal structures were used for total energy calculation of crystals, and the optimized molecular structures in salts ([Me₄N]₂[Ni(mnt)₂], [Et₄N]₂[Ni(mnt)₂], [Pr₄N]₂[Ni(mnt)₂] and [Bu₄N]₂[Ni(mnt)₂]), including [Ni(mnt)₂]²⁻, Me₄N⁺, Et₄N⁺,

PrN₄⁺, Bu₄N⁺, were used for their calculation of single point energy. The Perdew-Burke-Ernzerhof (PBE) function of generalized gradient approximation (GGA) was employed to represent the exchange-correlation energy in the electronic system precisely.⁸ Double numerical basis with orbital polarization function (DNP) was selected for both total energy calculation of crystals and single point energy calculations of individual anion/cation. During total energy calculation, a 1 × 1 × 1 Monkhorst-Pack grid of k-points were used to sample the Brillouin zone while permitting full structural relaxation and self-consistency.⁹ The energy and SCF convergence criteria are set to 1.0×10⁻⁵ Hartree and 1.0×10⁻⁶ with a global fixed to accelerate the convergence steps for total energy calculation of crystals.

The lattice formation energies (ΔE_{latt}) are calculated through Eq. (1),

$$\Delta E_{\text{latt}} = E_{\text{crystal}} - E_{\text{anion}} - E_{\text{cation-1}} - E_{\text{cation-2}} \quad (1)$$

where the symbols E_{latt} , E_{anion} , $E_{\text{cation-1}}$, and $E_{\text{cation-2}}$ represent the lattice formation energies, the total energies of crystal, the energies of components in crystal (anion and two cations), respectively.



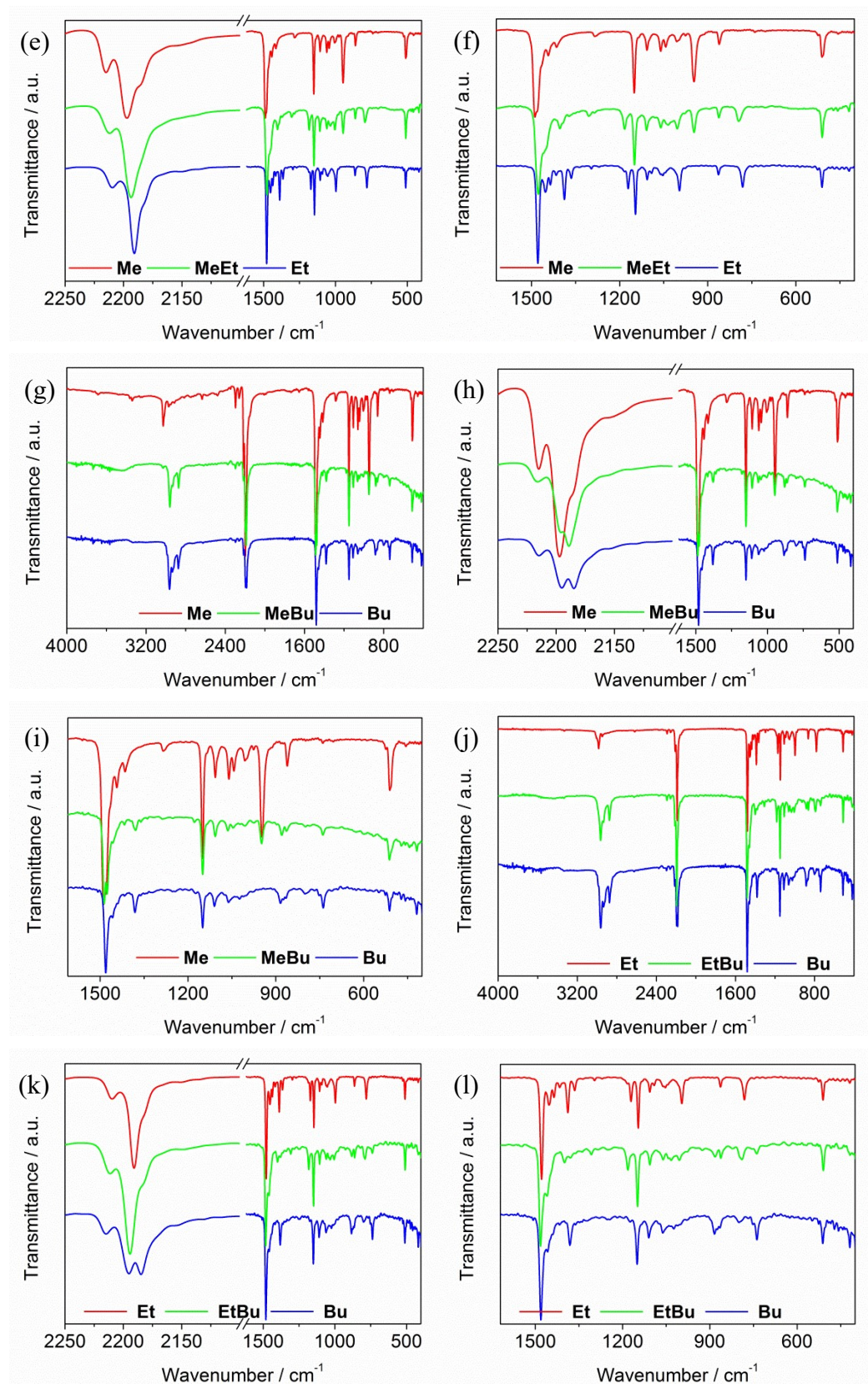


Figure S1: IR spectra of (a–c) **Me**, **Et**, **Pr** and **Bu**, (d–f) **Me**, **Et** and **MeEt**, (g–i) **Me**, **Bu** and **MeBu**, (j–l) **Et**, **Bu** and **EtBu**.

Table S3. Main vibrational bands and assignments in IR spectra of **Me, Et, Pr, Bu, MeEt, MeBu** and **EtBu**

Compound	Main vibrational band / cm^{-1} and assignments ¹⁰
Me	2965(s) assigned to $\nu_{\text{C-H}}$; 2198(vs) assigned to $\nu_{\text{C}\equiv\text{N}}$; 1488(vs) assigned to $\nu_{\text{C}=\text{C}}$; 1150(s) and 1061(s) assigned to $\nu_{\text{C-C}} + \nu_{\text{C-N}}$; 885(w) assigned to $\nu_{\text{C-S}}$
Et	2984(s) assigned to $\nu_{\text{C-H}}$; 2191(vs) assigned to $\nu_{\text{C}\equiv\text{N}}$; 1479(vs) assigned to $\nu_{\text{C}=\text{C}}$; 1146(s) and 1053(s) assigned to $\nu_{\text{C-C}} + \nu_{\text{C-N}}$; 941(w) assigned to $\nu_{\text{C-S}}$
Pr	2973(s) assigned to $\nu_{\text{C-H}}$; 2193(vs) assigned to $\nu_{\text{C}\equiv\text{N}}$; 1479(vs) assigned to $\nu_{\text{C}=\text{C}}$; 1149(s), 1046(s) assigned to $\nu_{\text{C-C}} + \nu_{\text{C-N}}$; 941(w) assigned to $\nu_{\text{C-S}}$
Bu	2965(s) and 2929(w) assigned to $\nu_{\text{C-H}}$; 2195(vs) assigned to $\nu_{\text{C}\equiv\text{N}}$; 1481(vs) assigned to $\nu_{\text{C}=\text{C}}$; 1078(s), 1050(s) assigned to $\nu_{\text{C-C}} + \nu_{\text{C-N}}$; 965(w) assigned to $\nu_{\text{C-S}}$
MeEt	2982(s) assigned to $\nu_{\text{C-H}}$; 2193(vs) assigned to $\nu_{\text{C}\equiv\text{N}}$; 1479(vs) assigned to $\nu_{\text{C}=\text{C}}$; 1107 (s), 1059(s) assigned to $\nu_{\text{C-C}} + \nu_{\text{C-N}}$; 946(w) assigned to $\nu_{\text{C-S}}$
MeBu	2960(s) and 2872(s) assigned to $\nu_{\text{C-H}}$; 2189(vs) assigned to $\nu_{\text{C}\equiv\text{N}}$; 1485(vs) assigned to $\nu_{\text{C}=\text{C}}$; 1108 (s), 1063(s) assigned to $\nu_{\text{C-C}} + \nu_{\text{C-N}}$; 949(w) assigned to $\nu_{\text{C-S}}$
EtBu	2964(s) and 2875(s) assigned to $\nu_{\text{C-H}}$; 2194(vs) assigned to $\nu_{\text{C}\equiv\text{N}}$; 1483(vs) assigned to $\nu_{\text{C}=\text{C}}$; 1107 (s), 1060(s) assigned to $\nu_{\text{C-C}} + \nu_{\text{C-N}}$; 882(w) assigned to $\nu_{\text{C-S}}$

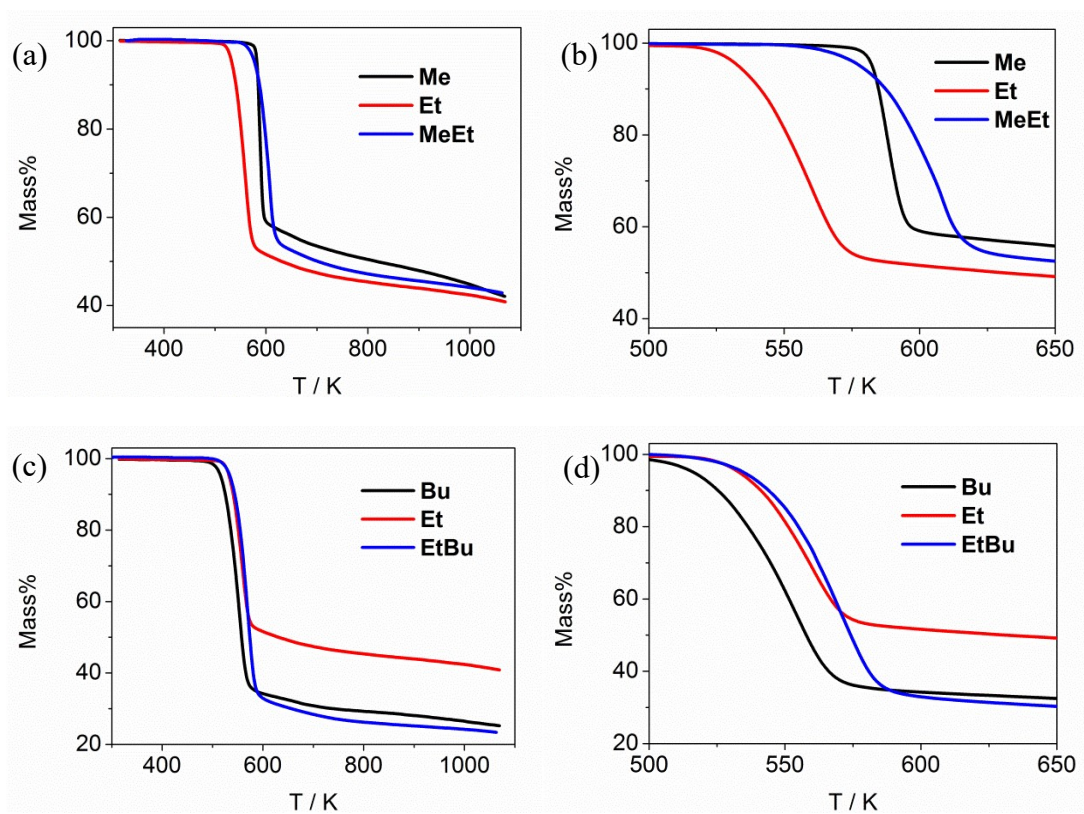


Figure S2: TG plots of (a, b) **Me**, **Et** and **MeEt**; (c) **Me**, **Bu** and **MeBu**; (c, d) **Et**, **Bu** and **EtBu**.

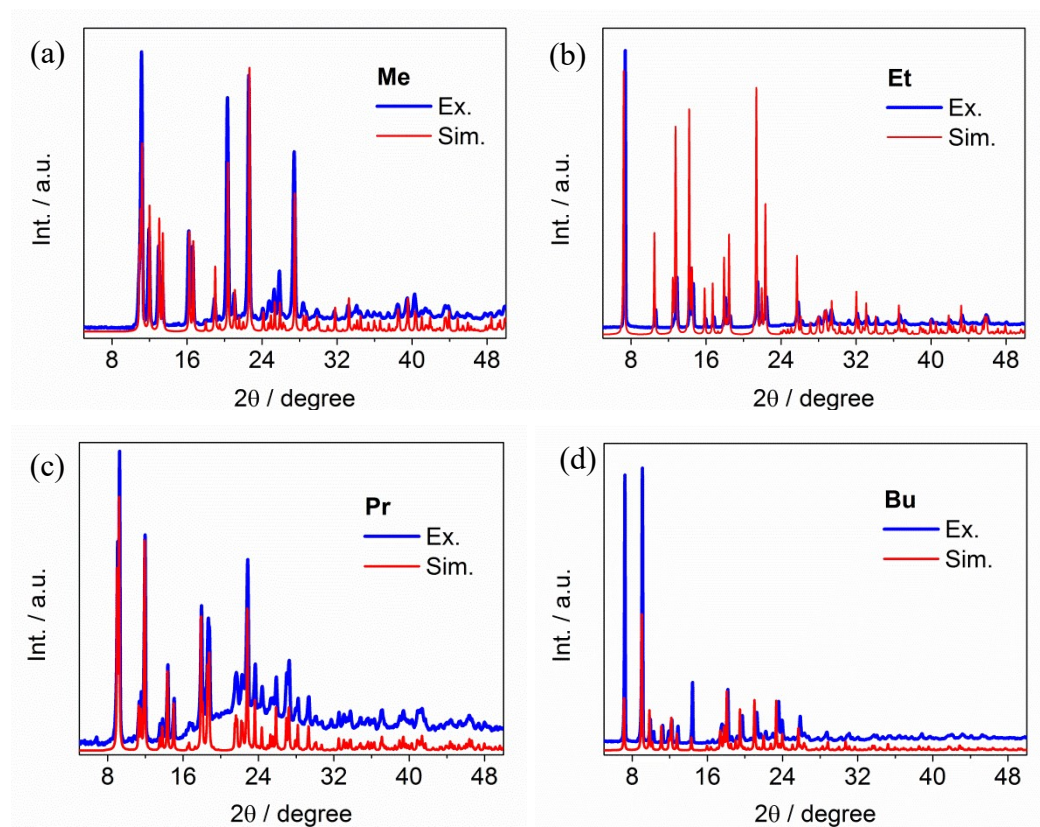


Figure S3. Experimental and simulated PXRD patterns of (a) **Me**, (b) **Et**, (c) **Pr**, (d) **Bu**. The simulated PXRD patterns of four salts are obtained from the corresponding single crystal diffraction data by Mercury 3.1 program. Experimental pattern matches well with the corresponding simulated one for each salt.

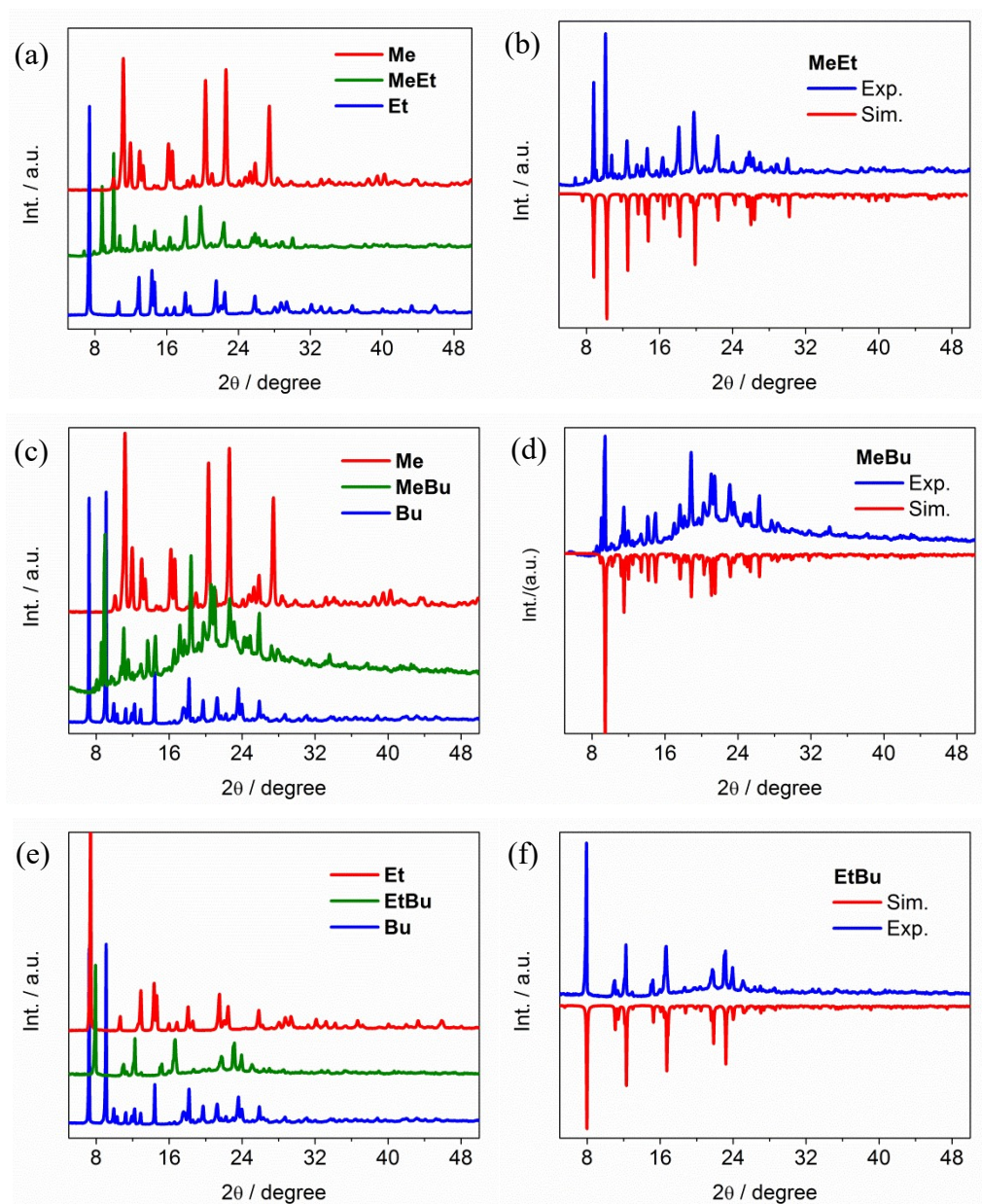


Figure S4. PXRD patterns of (a) **Me**, **Et** and **MeEt** (c) **Me**, **Bu** and **MeBu** (e) **Et**, **Bu** and **EtBu**. And experimental and simulated PXRD patterns of (b) **MeEt** (d) **MeBu** (f) **EtBu**. The simulated PXRD patterns of three co-crystals are acquired from the corresponding single crystal diffraction data by Mercury 3.1 program. Experimental pattern matches well with the corresponding simulated one for each co-crystal.

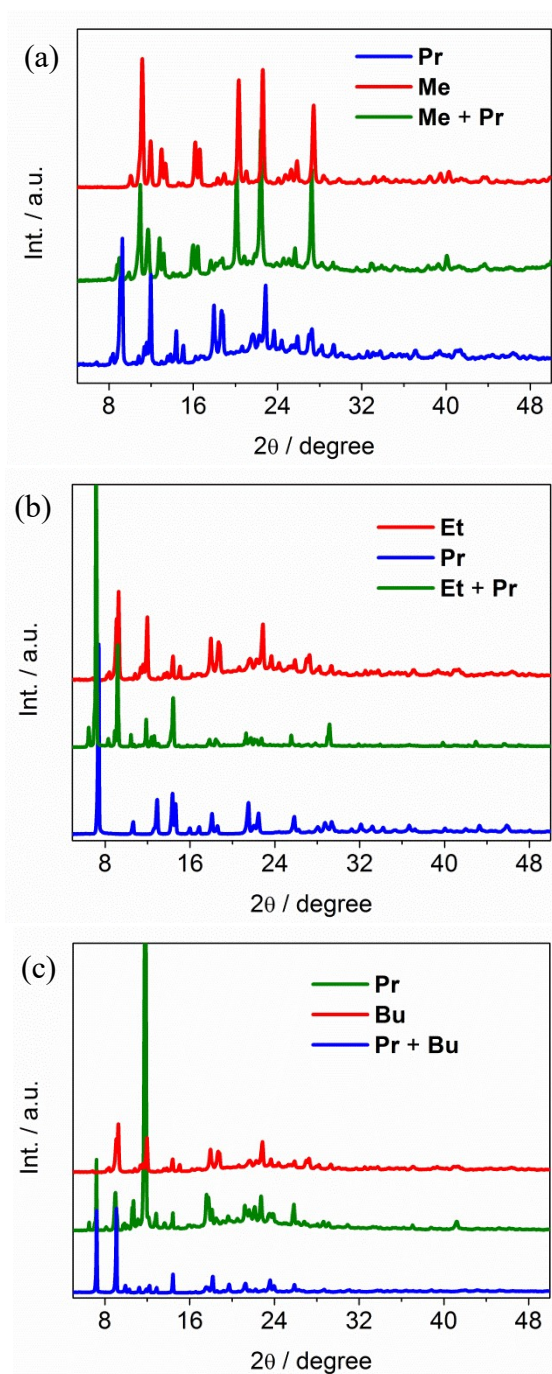


Figure S5. PXR D patterns of (a) Me, Pr and Me+Pr (b) Et, Pr and Et+Pr (c) Pr, Bu and Pr+Bu, in which Me+Pr represents the crystalline sample obtained by slow evaporation the solution of Me and Pr with equal mole ratio; the symbols, Et+Pr and Pr+Bu, show similar meanings, and the details refer to the main text.

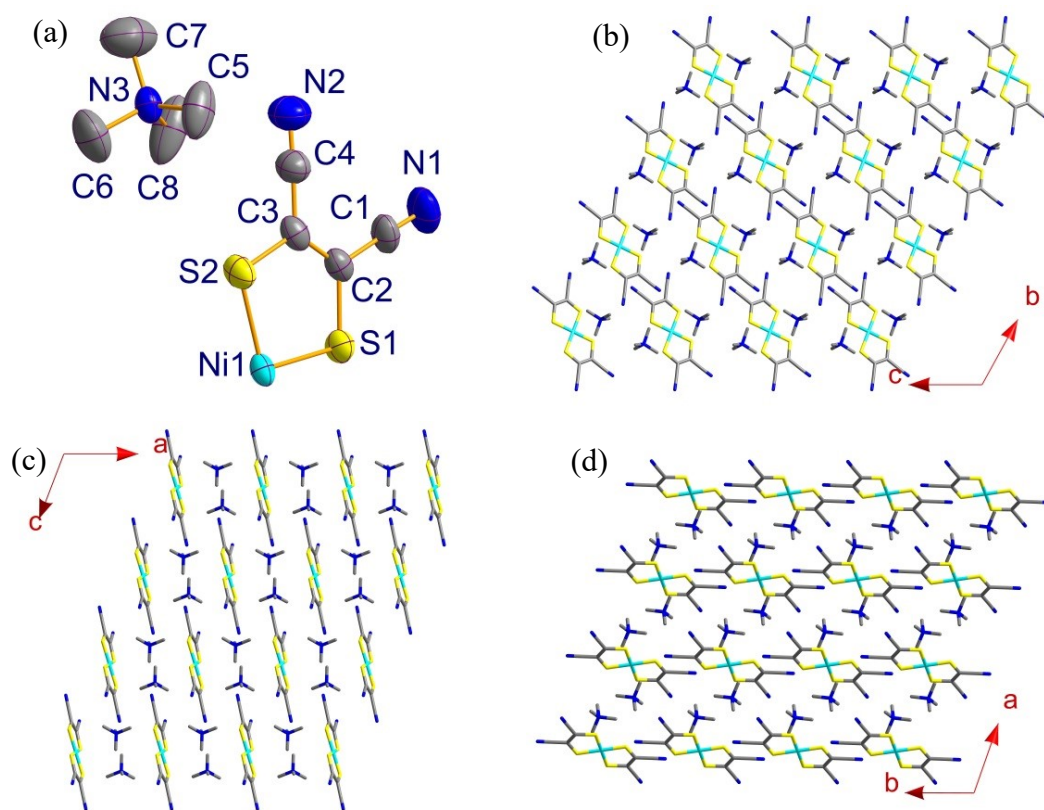


Figure S6. (a) Asymmetric unit (where the displacement ellipsoids are drawn at 50% probability level for non-hydrogen atoms, and hydrogen atoms are omitted for clarity), and packing diagrams of viewed along (b) a-axis (c) b-axis (d) c-axis for **Me**.

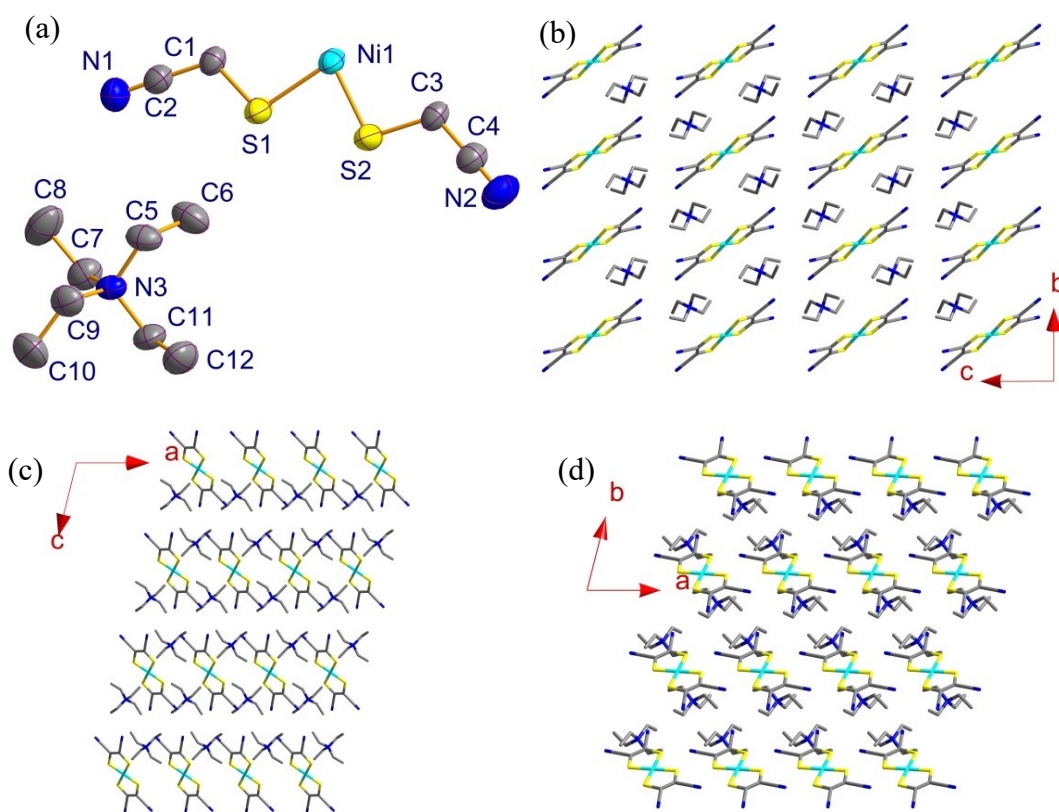


Figure S7. (a) Asymmetric unit (where the displacement ellipsoids are drawn at 50% probability level for non-hydrogen atoms, and hydrogen atoms are omitted for clarity), and packing diagrams of viewed along (b) a-axis (c) b-axis (d) c-axis for **Et**.

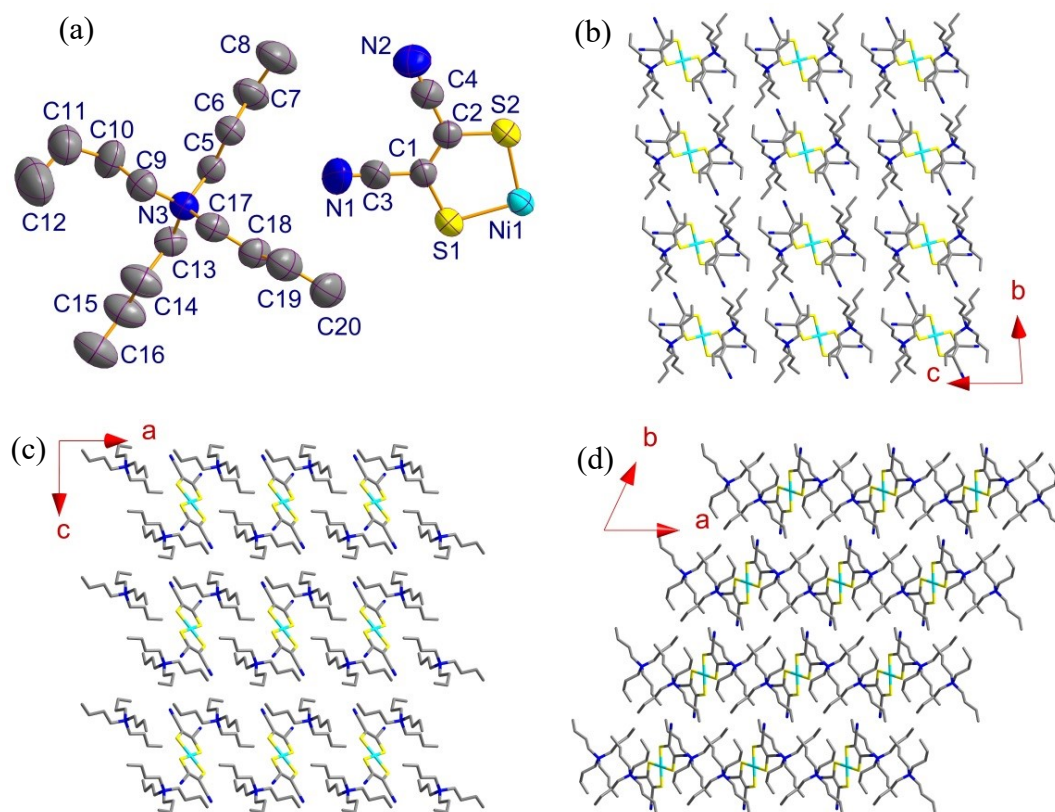


Figure S8. (a) Asymmetric unit (where the displacement ellipsoids are drawn at 50% probability level for non-hydrogen atoms, and hydrogen atoms are omitted for clarity), and packing diagrams of viewed along (b) a-axis (c) b-axis (d) c-axis for **Et**.

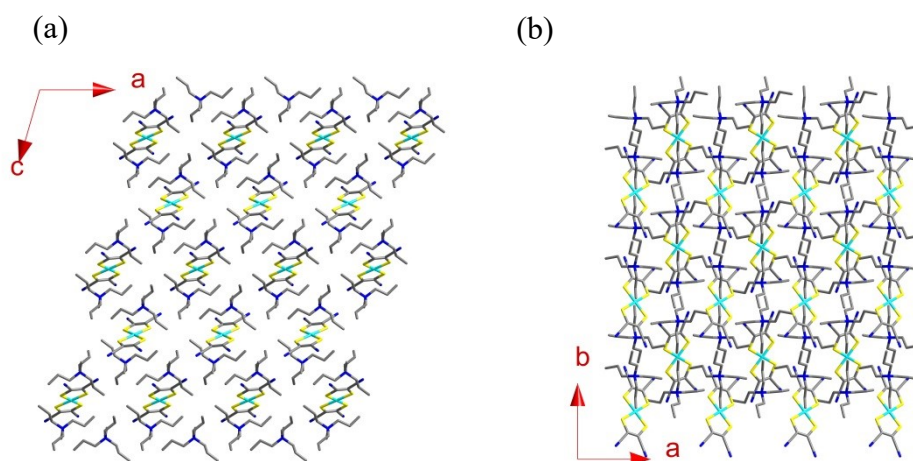


Figure S9. Packing diagrams of viewed along (a) b-axis and (d) c-axis for **Pr**.

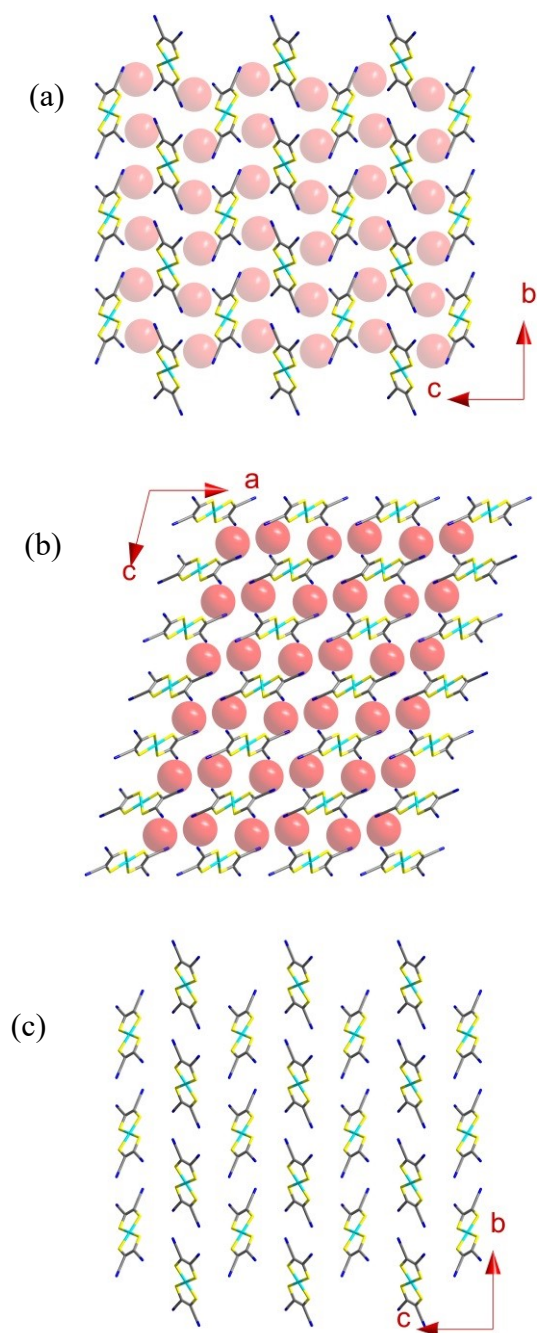


Figure S10. Packing diagrams in **MeEt** viewed along (a) a-axis and (b) b-axis; (c) anion monolayer in **MeEt** viewed along a-axis.

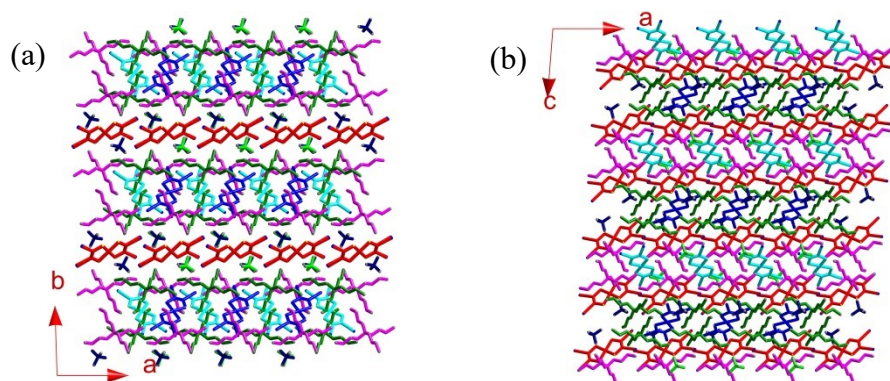


Figure S11. Packing diagrams of viewed along (a) c-axis and (d) b-axis for **MeBu**.

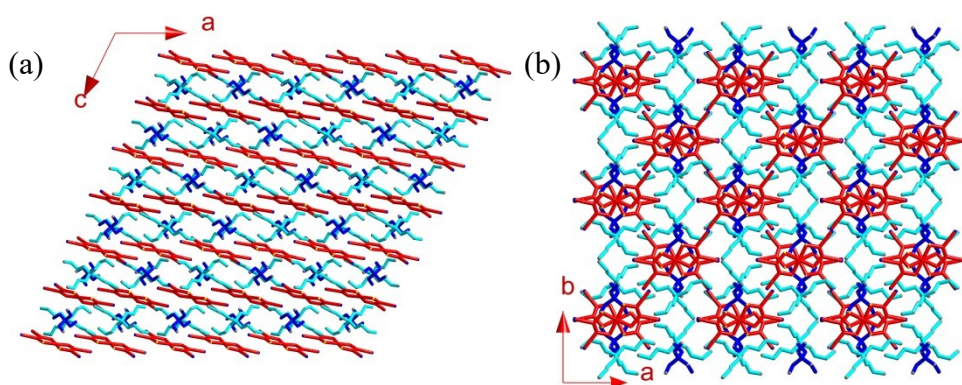


Figure S12. Packing diagrams of viewed along (a) b-axis and (b) c-axis for **EtBu**.

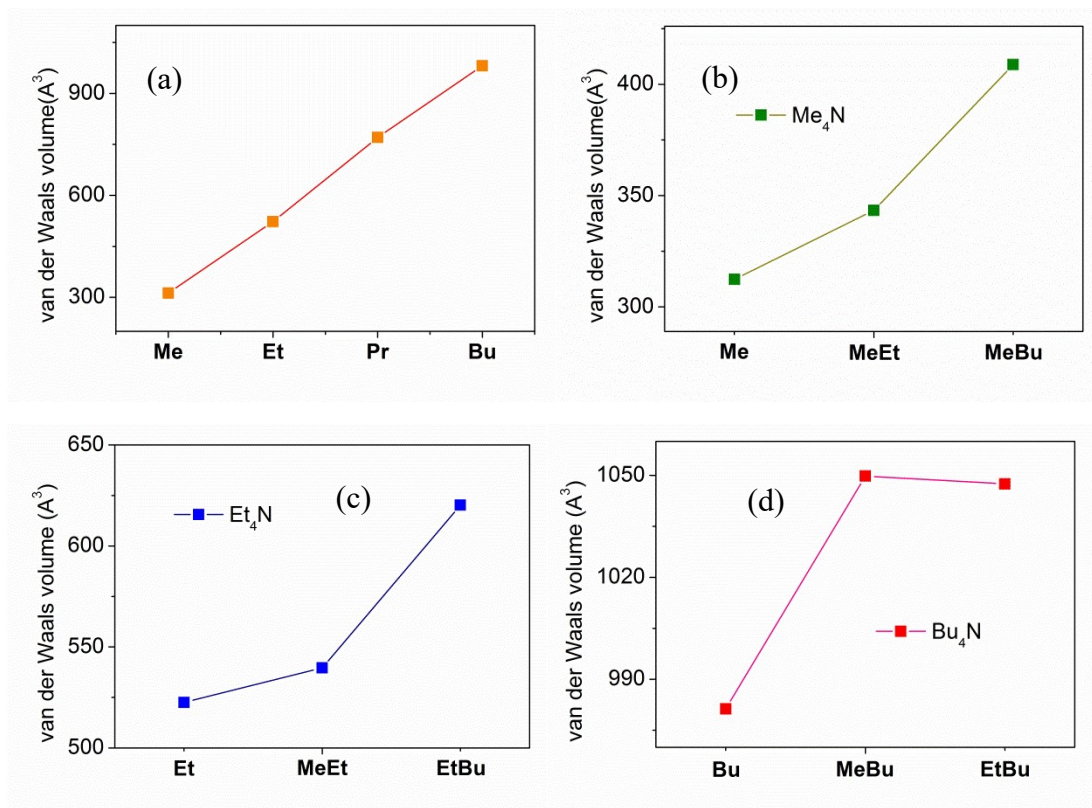


Figure S13. Plots of (a) van der Waals volume per cation, which was obtained by PLATON program, in (a) **Me**, **Et**, **Pr** and **Bu**; (b) **Me₄N⁺** in **Me**, **MeEt**, **MeBu**; (c) **Et₄N⁺** in **Et**, **MeEt** and **EtBu**; (d) **Bu₄N⁺** in **Bu**, **MeBu** and **EtBu**; (e) van der Waals volume per anion in **Me**, **Et**, **Pr**, **Bu**, **MeEt**, **MeBu** and **EtBu**.

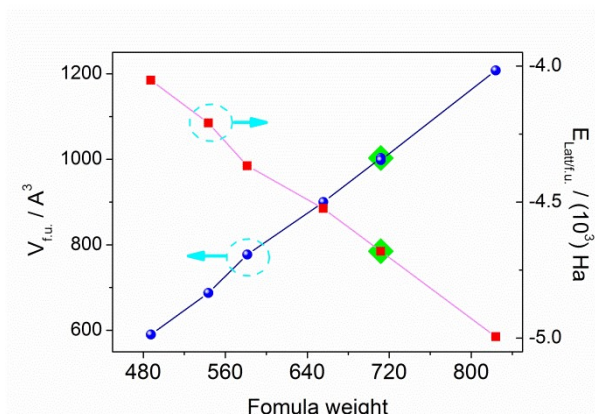


Figure S14. Plots of $V_{f.u.}$ and $E_{Latt/f.u.}$ against formula weight for **Me, Et, Pr, Bu, MeEt, MeBu** and **EtBu**, where the green diamond \blacklozenge in two plots represent the $V_{f.u.}$ and $E_{Latt/f.u.}$ of **Pr**.

Table S4. Comparison of crystal volume per formula unit and crystal energy per formula unit of a cocrystal with its two corresponding salts

Herein,

$$\Delta V_{f.u.} =$$

$$V_{f.u.}([Cat_1][Cat_2][Ni(mnt)_2]) - \{V_{f.u.}([Cat_1]_2[Ni(mnt)_2]) + V_{f.u.}([Cat_2]_2[Ni(mnt)_2])\} / 2$$

$$\Delta E_{f.u.} =$$

$$E_{f.u.}([Cat_1][Cat_2][Ni(mnt)_2]) - \{E_{f.u.}([Cat_1]_2[Ni(mnt)_2]) + E_{f.u.}([Cat_2]_2[Ni(mnt)_2])\} / 2$$

Cat_1, Cat_2	$V_{f.u.}([Cat_1][Cat_2][Ni(mnt)_2])$ / \AA^3	$\{V_{f.u.}([Cat_1]_2[Ni(mnt)_2])$ $+ V_{f.u.}([Cat_2]_2[Ni(mnt)_2])\} / 2$ / \AA^3	$\Delta V_{f.u.}$ / \AA^3
Me, Et	687.61(7)	683.62(3)	3.99(3)
Me, Bu	900.10(2)	898.99(3)	1.11(2)
Et, Bu	997.93(2)	992.42(3)	5.51(2)

Cat_1, Cat_2	$E_{f.u.}([Cat_1][Cat_2][Ni(mnt)_2])$ / eV	$\{E_{f.u.}([Cat_1]_2[Ni(mnt)_2])$ $+ E_{f.u.}([Cat_2]_2[Ni(mnt)_2])\} / 2$ / eV	$\Delta E_{f.u.}$ / eV
Me, Et	-7915.7675	-7915.9264	0.1589
Me, Bu	-9436.0922	-9436.1236	0.0314
Et, Bu	-10196.4932	-10196.4956	0.0024

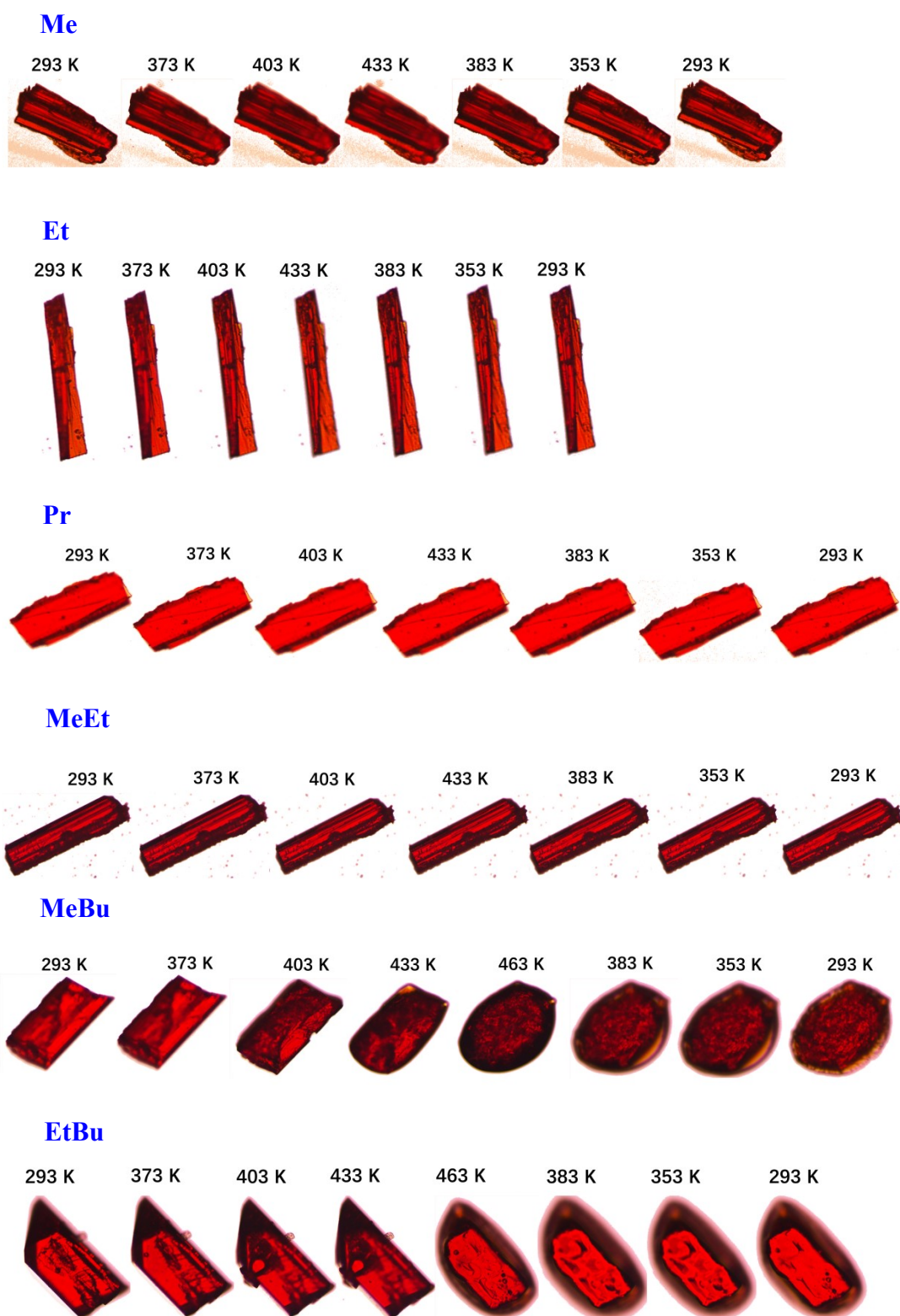


Figure S15. Variable temperature crystal morphologies of **Me**, **Et**, **Pr**, **MeEt**, **MeBu** and **EtBu**.

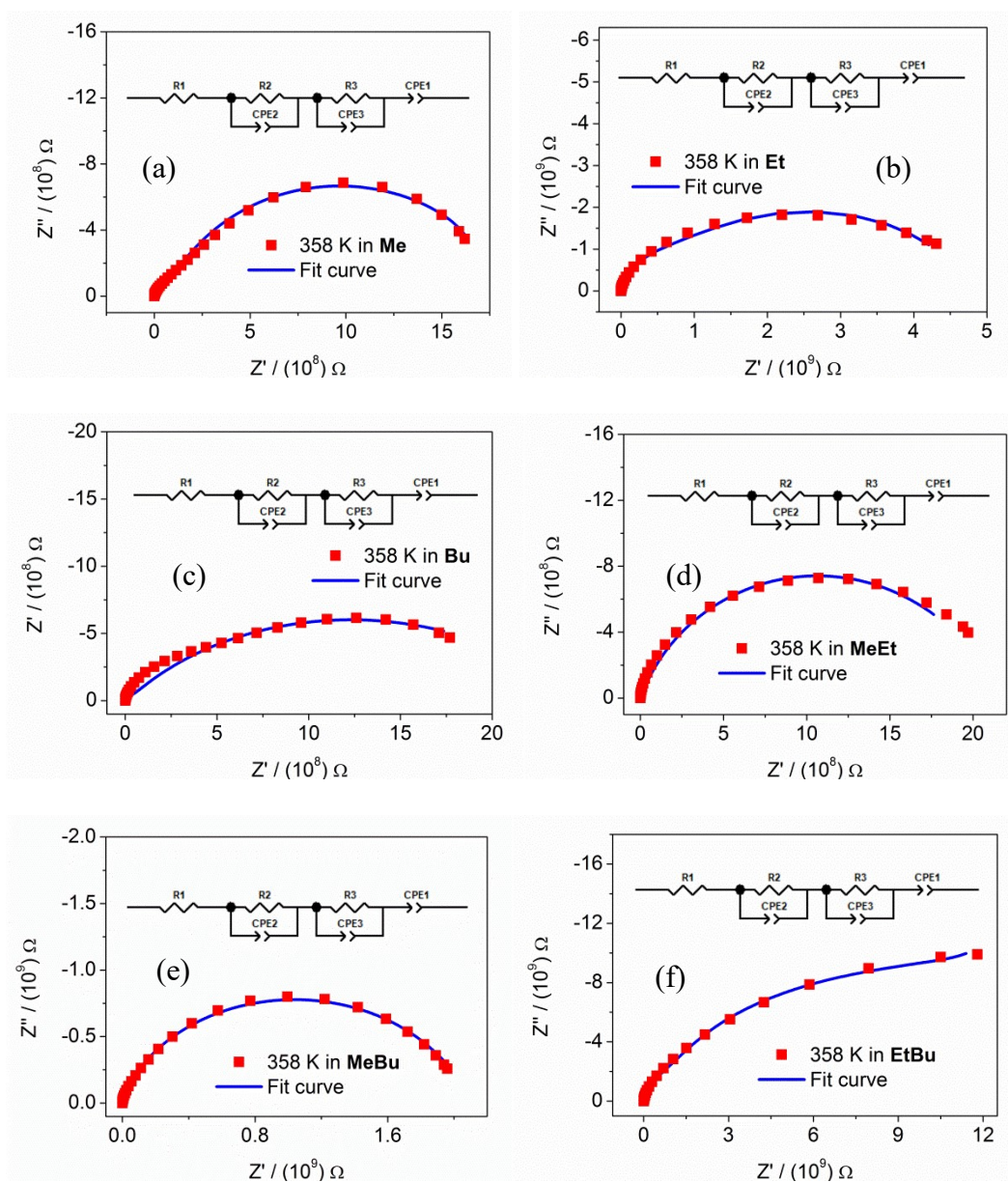


Figure S16. Impedances at 358 K together with the corresponding fit curves using the equivalent circuit (insets) for (a) Me, (b) Et, (c) Bu, (d) MeEt, (e) MeBu and (f) EtBu.

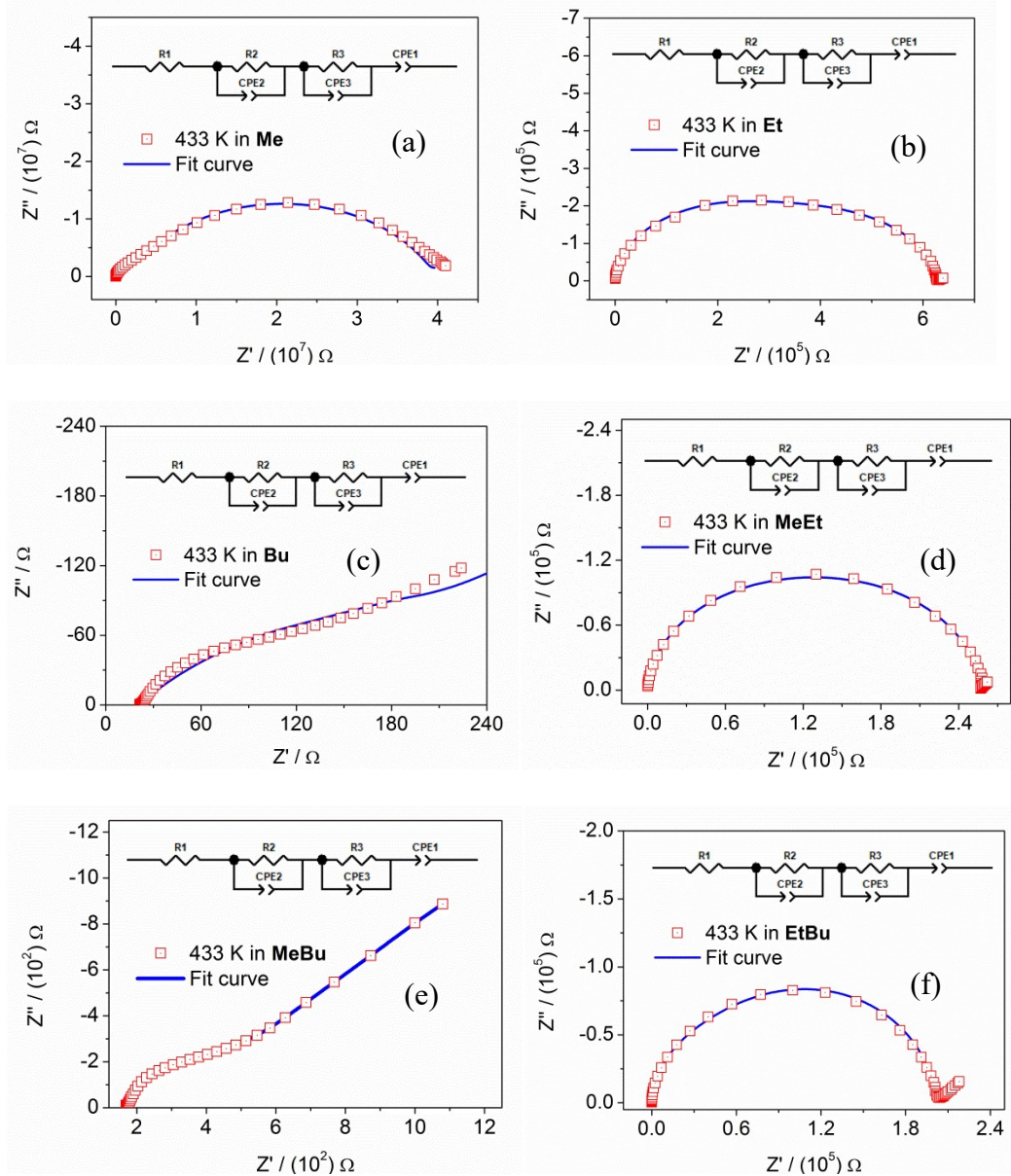


Figure S17. Impedances at 433 K together with the corresponding fit curves using the equivalent circuit (inset) for (a) **Me**, (b) **Et**, (c) **Bu**, (d) **MeEt**, (e) **MeBu** and (f) **EtBu**.

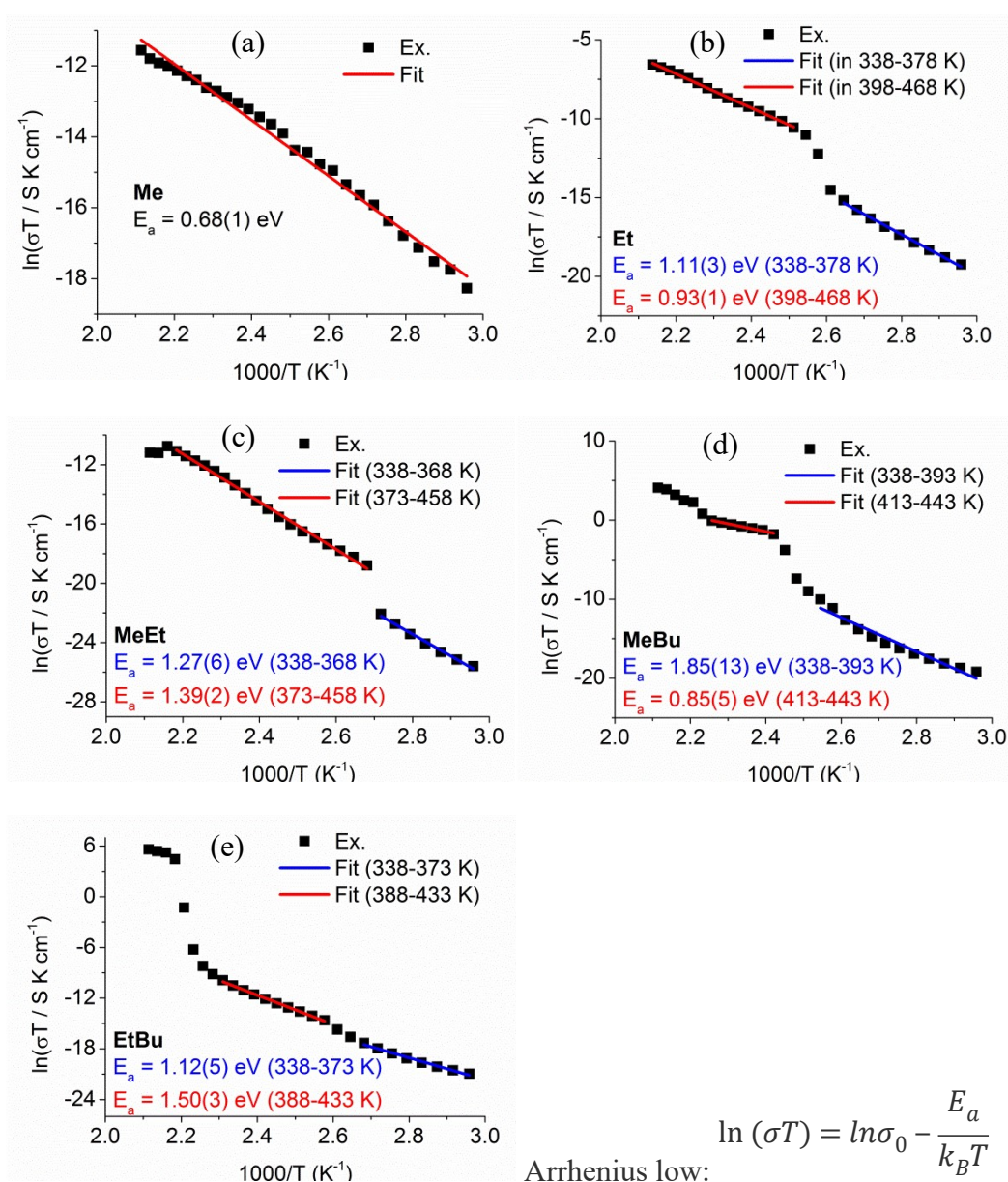


Figure S18. Arrhenius plots together with the corresponding linear fits and activation energies for (a) **Me**, (b) **Et**, (c) **MeEt**, (d) **MeBu** and (e) **EtBu**.

References

1. A. Davidson and H. R. Holm, Metal Complexes Derived from Cis-1, 2-Dicyano-1, 2-Ethylenedithiolate and Bis(trifluoromethyl)-1,2-Dithiete, *Inorg. Synth.*, 1967, **10**, 8–26.
2. R. Eisenberg and J. A. Ibers, Structure of Di(tetramethylammonium) Bis(maleonitriledithiolate)nickelate(II), *Inorg. Chem.*, 1965, **4**, 605–608.
3. A. Kobayashi and Y. Sasaki, One-dimensional System of Square-planar Bis(1, 2-dicyanovinylene-1, 2-dithiolato)metal Complexes. I. the Crystal Structure of $[(C_4H_9)_4N]_2[Ni(mnt)_2]$ and $[(C_2H_5)_4N][Ni(mnt)_2]$, *Bull. Chem. Soc. Jpn.*, 1977, **50**, 2650–2656.
4. Bruker, *APEX 2*, *SAINT*, *XPREP*, Bruker AXS Inc., Madison, Wisconsin, USA, 2007.
5. Bruker, *SADABS*, Bruker AXS Inc., Madison, Wisconsin, USA, 2001.
6. G. M. Sheldrick, *SHELXS-2014*, Program for the Solution and Refinement of Crystal Structures, University of Göttingen, Göttingen, Germany, 2014.
7. B. Delley, From Molecules to Solids with the DMol³ Approach, *J. Chem. Phys.*, 2000, **113**, 7756–7764.
8. J. P. Perdew, K. Burke and Ernzerhof, M. Generalized Gradient Approximation Made Simple, *Phys. Rev. Lett.*, 1996, **77**, 3865–3868.
9. H. J. Monkhorst, and J. D. Pack, Special Points for Brillouin-zone Integrations, *Phys. Rev. B*, 1976, **13**, 5188–5192.
10. C. W. Schläpfer, and K. Nakamoto, Infrared Spectra and Normal-Coordinate Analysis of 1,2-Dithiolate Complexes with Nickel, *Inorg. Chem.*, 1975, **14**, 1338–1344.